The mechanism of Al donor defects in (Zn, Co)O:Al: a view from resonant x-ray spectroscopies

2009 J. Phys.: Condens. Matter 21 495502

(http://iopscience.iop.org/0953-8984/21/49/495502)

J. Phys.: Condens. Matter **21** (2009) 495502 (7pp) doi:10.1088/0953-8984/21/49/495502

The mechanism of Al donor defects in (Zn, Co)O:Al: a view from resonant x-ray spectroscopies

K J Zhou[1,5], Y Tezuka[2], M Q Cui[1], J Zhao[3], X C Liu[4], Z Z Chen[4] and Z Y Wu[1]

[1] Beijing Synchrotron Radiation Facility, Institute of High Energy Physics, Beijing 100049, People's Republic of China
[2] Department of Advanced Physics, Faculty of Science and Technology, Hirosaki University, Aomori, 036-8561, Japan
[3] Mathematics and Physics Department, Beijing Technology and Business University, Beijing 100037, People's Republic of China
[4] Shanghai Institute of Ceramics, Chinese Academy of Sciences, Shanghai 200050, People's Republic of China

E-mail: kejin.zhou@psi.ch

Received 6 May 2009, in final form 30 September 2009
Published 12 November 2009
Online at stacks.iop.org/JPhysCM/21/495502

Abstract

We studied the effect of Al doping in $Zn_{0.94}Co_{0.05}Al_{0.01}O$ nano-powders from the electronic structure point of view by applying x-ray absorption spectroscopy and resonant inelastic x-ray scattering at the oxygen K- and Co L-edges. The intensity of the pre-edge structure of the O-K XAS spectra is enhanced following the introduction of the Al defect. Multiple scattering calculations demonstrate it can be accounted for by the gain of the hybridization strength between O 2p and Al 3p (and/or Co 3d) states. The consensus on the hybridization strength is reached by combining Co-L XAS and RIXS investigations and multiplet calculations. It reveals different spatial substitutions of Al doping can alter the number of shared oxygen atoms between the Co and Al tetrahedrons. These shared ligands are responsible for the Al 3p and Co 3d state hybridization strength as well as the ferromagnetism of the ground state. The magnetic difference is better understood to be governed by various shared oxygen atoms rather than the distance between the Al defect and Co impurities.

(Some figures in this article are in colour only in the electronic version)

1. Introduction

A long-pursued goal among quantum spintronics is manipulating the spin degree of freedom of charges at room temperature (RT) in order to boost both the speed and the storage capacity of the microelectronic devices. Interest in discovering the mechanism of the ferromagnetism (FM) of these materials as well as their fabrication has been increasingly stimulated since the success of creating FM at RT by doping Co into ZnO [1–3]. Soon after, RT FM was found to be present in other 3d transition metal doped oxides such as Cr:TiO_2, Mn:ZnO, etc [4, 5]. Recent explorations on Co doped ZnO showed that FM can be facilitated upon the doping of additional impurities such as Cu, Al or Ga [6–8]. Even Al doped ZnO without Co can possess RT FM [9]. Post-treatment, such as film annealing under a hydrogen environment, also promotes RT FM [10]. In spite of these promising findings, contradictory magnetic properties ranging from paramagnetic, antiferromagnetic to spin-glass behavior were also reported in (Zn, Co)O [11, 12]. These reporters believe that the ferromagnetism must somehow be associated with clustering or precipitates as a secondary ferromagnetic phase, although divalent cobalt substituting Zn sites reported by other spectroscopic studies [13, 14]. In our recent investigations on (Zn, Co)O thin films [15, 16], we noted that both oxygen vacancies (V_O) and co-doped free carriers such as Al contribute as donor defects and assist RT FM.

[5] Author to whom any correspondence should be addressed. Present address: Paul Scherrer Institut, Swiss Light Source, Switzerland.

Moreover, magnetization measurements and x-ray absorption spectroscopy studies indicated that the oxygen deficient growth conditions promote ferromagnetism in thin films [15]. So far, understanding the magnetic mechanism of Co doped ZnO is still far from being complete. This is because normally ferromagnetism, which resides in n-type conditions, cannot be simply explained by the typical hole-mediated p–d Zenel model [17].

Our recent first-principles DFT calculations reported that the additional electrons induced by Al doping in (Co, Al) co-doped ZnO can stabilize the ferromagnetic state and the magnetic ground state energy is significantly changed due to different doping positions of Al [18]. However, we did not thoroughly understand why different Al substitutional sites induce various magnetic ground state energies. Since the Co 3d and Al 3p hybridized states vary as well upon different doping sites, we propose to investigate the mechanism, especially the hybridization strength, from the electronic structure point of view through x-ray absorption spectroscopy (XAS) and resonant inelastic x-ray scattering (RIXS) at the oxygen K-edge and Co L-edges, supported by *ab initio* multiple scattering and multiplet calculations. Nano-powder samples, $Zn_{0.95}Co_{0.05}O$ and $Zn_{0.94}Co_{0.05}Al_{0.01}O$ are chosen to exclude one of the magnetic contributions from oxygen vacancies. This simplifies the exploration of the mechanism of co-doped Al donor defects, since normally oxygen vacancies are generated through a deficient oxygen environment. Our previous magnetic measurements signified that $Zn_{0.95}Co_{0.05}O$ is paramagnetic and $Zn_{0.94}Co_{0.05}Al_{0.01}O$ presents room temperature ferromagnetism. Co ions have been verified to substitute Zn sites in both samples [7]. The local electronic structures through the x-ray spectroscopic studies are expected to deliver plentiful information on the electronic mechanism of Al donor defects.

2. Experimental details

Nano-powder samples, $Zn_{0.95}Co_{0.05}O$ and $Zn_{0.94}Co_{0.05}Al_{0.01}O$, were fabricated by the sol–gel process. Hereafter, they are designated as ZCO and ZCAO respectively for simplification. Details about the sample preparation and magnetic measurements are referred to [7]. XAS and RIXS spectra at both O K- and Co L-edges were collected at the BL-2C beam line of Photon Factory in the High Energy Accelerator Research Organization (KEK-PF, Japan). The beam from an undulator is monochromatized by a self-focusing varied-space plane grating [19]. The x-ray absorption data were recorded from the sample using drain current. The photon energy of the beam line was calibrated according to the Au 4f photoemission peak. RIXS experiments were performed at a high resolution grazing incidence grating spectrometer equipped with a two-dimensional position-sensitive detector [20]. The emission energy was calibrated according to the fluorescence of Co metal. The energy resolution of the monochromator was about 0.2 eV and 0.5 eV during XAS and RIXS measurements, respectively. The incoming beam was linearly polarized in the horizontal scattering plane. The RIXS signal was detected at a scattering angle of 90° with respect to the incident photons, which impinged on the sample surface with a grazing angle of 20°. All measurements were carried out at room temperature.

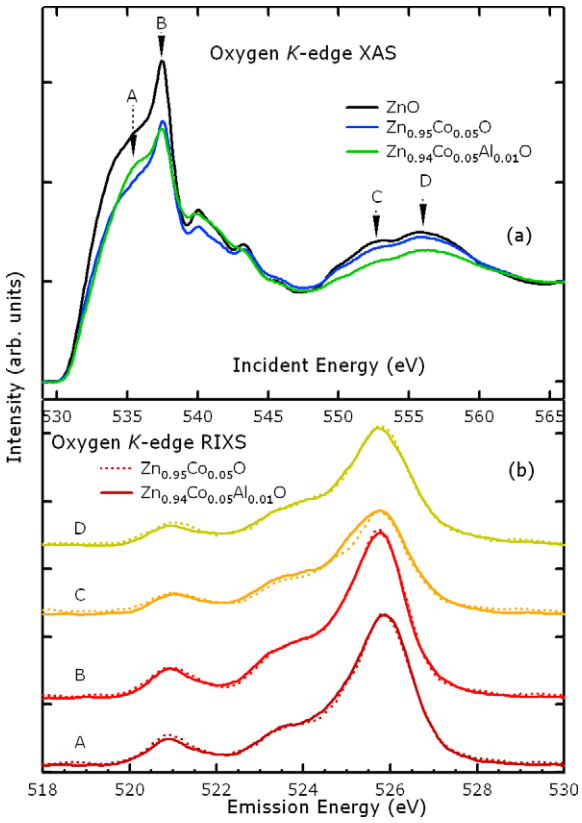

Figure 1. (a) O-K XAS spectra of ZnO, ZCO and ZCAO. (b) O-K RIXS spectra under the excitation energy A, B, C, and D.

3. Results and discussions

3.1. Oxygen K-edge

Figure 1(a) illustrates the O K-edge XAS spectra of ZCO, ZCAO as well as that of the ZnO reference. A decrease of the intensities of features A–D was observed in both samples compared with the ZnO reference. This is in line with the results of $Zn_{1-x}Co_xO$ reported by Chiou *et al*, who explained that the low intensity, especially of the white line, is caused by the electron transfer from the Co dopant to O 2p states [21]. Further investigations on feature A signified ZCAO holds a stronger intensity than ZCO while the others are less intense following the Al doping. As in general feature A contains the information of the hybridization between O 2p and Co 3d states, the difference denotes that the additional doped Al defect drives the modification of the hybridization strength. It was known that in our case the oxygen vacancies can be excluded since both samples have been sintered at a high temperature for several hours [7]. We therefore question how the Al defects alter the electronic structure of feature A. For the sake of the systematic investigation of the Al doping effect, multiple scattering O-K XAS calculations are then performed through the FEFF8.2 code [22], as O-K XAS obeys the band structure theory. We employ a self-consistent

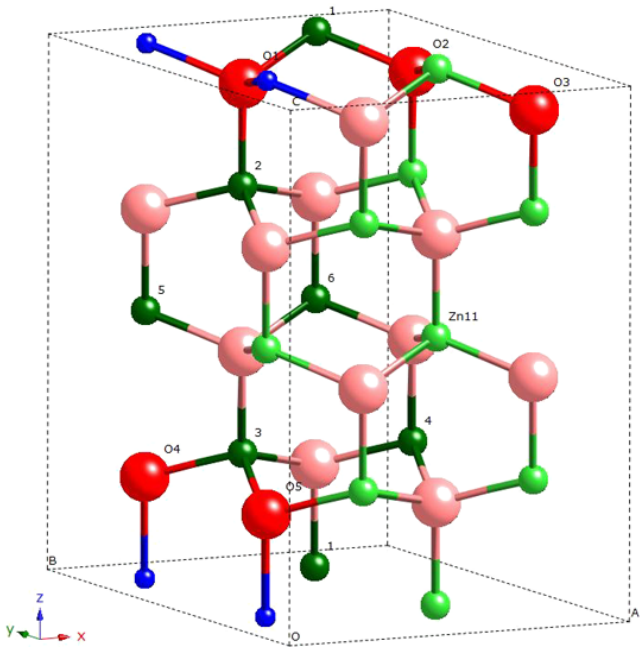

Figure 2. Wurtzite ZnO supercell (2 × 2 × 2). Green, blue, and red spheres represent Zn, Co, O ions respectively. The dark green spheres are the different Zn sites substituted by Al ions and labeled as 1 to 6. The shared oxygens between Co and Al tetrahedrons are illustrated by dark red spheres and labeled as O_1 to O_5. Zn_{11} is another Al substitutional site in addition to sites 1–6.

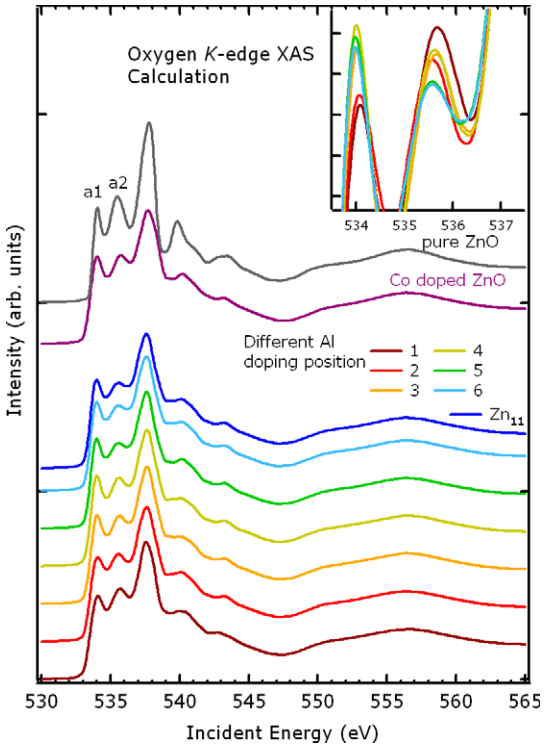

Figure 3. Calculated O-K XAS results. The upper two are that of pure ZnO and Co doped ZnO, respectively. The lower part includes the spectra when Al doping from site 1 to 6 and the one when Al substitutes Zn_{11}.

and fully relaxed core-hole potential as well as the Hedin and Lundqvist model. A 2 × 2 × 2 supercell geometry containing 32 atoms is constructed and displayed in figure 2. Two Co dopings are put continuously along the *ob* direction since the antiferromagnetic ground state was calculated to be stabilized in this configuration [23]. The structure was fully force-relaxed by optimizing the total energy. In order to compare this with the electronic structure retrieved from the previous DFT calculations [18], Al substitution is varied from site 1 to 6 in exactly the same way as was done before.

Figure 3 presents the calculated O-K XAS spectra of pure ZnO, ZCO, as well as ZCAO with different Al doping sites. The calculated results agree fairly well with the experimental data. The intensities of features A and B of ZCO are evidently lower than those of pure ZnO. In addition, due to the higher energy resolution included, feature A is better resolved as two peaks which are labeled by a1 and a2. A further comparison of a1 and a2 is made in the inset of figure 3. It seems that feature a1 gains intensity when the Al doping moves from site 3 to 6, while feature a2 shows the inverse tendency.

We correlate the difference of a1 and a2 to various hybridization strengths between O 2p and Al 3p (and/or Co 3d) unoccupied states. XAS calculations show the oxygen atoms of the nearest neighbor (NN) of the Al and Co ions providing distinct line shapes from the others, which is understandable as Al 3p and Co 3d states hybridize directly with 2p states of these NN ligands. Investigation on the shared oxygen atoms between Al and Co tetrahedrons denotes its number varies when Al substitutes different Zn positions. To differentiate the shared oxygen atoms with unshared ones, they are plotted as dark red spheres and labeled with O_n ($n = 1$, 2, etc) in the supercell of figure 2. For instance, when Al substitutes site 1, there are three oxygen atoms (O_1, O_2, O_3) belonging to both tetrahedrons. While when Al substitutes site 2, there is only one shared oxygen atom O_1. For sites 3 and 4, two oxygen atoms (O_4 and O_5) and one oxygen atom (O_4) are shared, respectively. No oxygen atom is owned by both tetrahedrons when Al in sites 5 and 6. It is clear that the number of shared oxygen atoms decreases from site 1 to 6, which in turn weakens the Al 3p and Co 3d hybridization strength. Thus a greater portion of free electrons likely dope into the host of ZnO matrix and enhance the hybridization strength between O 2p and Al 3p (and/or Co 3d) states. To verify the inference, we add up and average the XAS spectra of the NN oxygen atoms. We find the intensity of feature A does increase from site 1 to 6, as shown in figure 4. From the DFT calculation, we know the system prefers the ferromagnetic ground state when Al substitutes site 5 or 6. This indicates the ferromagnetic ground state of ZCAO favors strong Al 3d (and/or Co 3d) and O 2p state hybridization strengths.

Besides O-K XAS, we carried out O-K RIXS studies especially when the excitation energy detuned to altered features. Figure 1(b) depicts O-K RIXS experimental spectra. From the RIXS studies on ZnO [24], the excitation around 521 eV is allocated to the hybridized states between Zn 3d and O 2p. We find it is slightly less intense after Al doping. Meanwhile, the O 2p valence band around 526 eV appears a little broader following the Al doping. Interestingly, the same broadening effect was also revealed from O-K RIXS

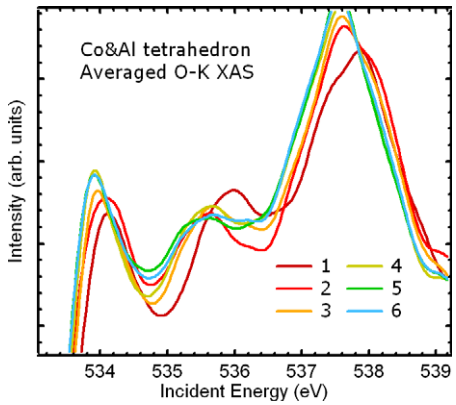

Figure 4. Calculated O-K XAS pre-edge structure of the oxygen atoms which belong to both Co and Al tetrahedrons when Al doping from site 1 to 6.

studies when Mn doping into ZnO [5]. The broadening there was attributed to the Mn doping and the O 2p and Mn 3d hybridization. Therefore, we consider the subtle variation of the O 2p valence band in ZCAO is probably induced by the enhancement of the hybridization strength between O 2p and Co 3d due to free carriers doped by Al defects.

3.2. Co L-edge

The Co $L_{2,3}$-edges XAS spectra of Co metal, ZCO and ZCAO are displayed in figure 5(a) as well as that of $Zn_{0.9}Co_{0.1}O$ from [25]. Comparison shows the majority of Co ions in both samples are divalent (+2), as was revealed by the previous Co K-edge EXAFS studies on the same system [7]. This properly manifests the carriers introduced by Al defects tend to form free electrons and are unlikely to localize around Co ions. In contrast to various O K-edge XAS spectra, Co $L_{2,3}$-edges present almost no difference between ZCO and ZCAO, except that the intensity of the charge transfer (CT) satellite (around ∼784 eV) gets slightly enhanced in the latter. This denotes the local crystal field strength of Co ions is preserved after introducing Al defects, while one of the hybridization strength V_{eg} (V_{t2g}) between oxygen 2p and Co 3d e_g (t_{2g}), the on-site Coulomb interaction U, and the CT energy Δ (the energy difference of the center of gravity between $3d^7$ and $3d^8\underline{L}$ configurations) is regulated following the Al doping.

For a better understanding of the fine structure of CT in XAS spectra, we carried out multiplet calculations using charge transfer multiplet (CTM) theory, as mostly the 3d transition metal L-edge XAS are governed by the excitonic and multiplet transitions. The channel from $3d^7 + 3d^8\underline{L}$ to $2p^5 3d^8 + 2p^5 3d^9\underline{L}$ is considered [26]. Here $\underline{L}$ implies a hole in the oxygen 2p valence band. The crystal field splitting (10 Dq), the charge transfer energy, and the hybridization are included. We find the experimental spectra can be well described with 10 Dq equal to −0.55 eV, as Co ions are located in a local T_d symmetry. To simulate the CT structure, we take into account the influences from the CT energy (Δ) and the Coulomb interaction (U), since the hybridization was established as not affecting the CT spectral shape [27]. Figure 5(b) shows the

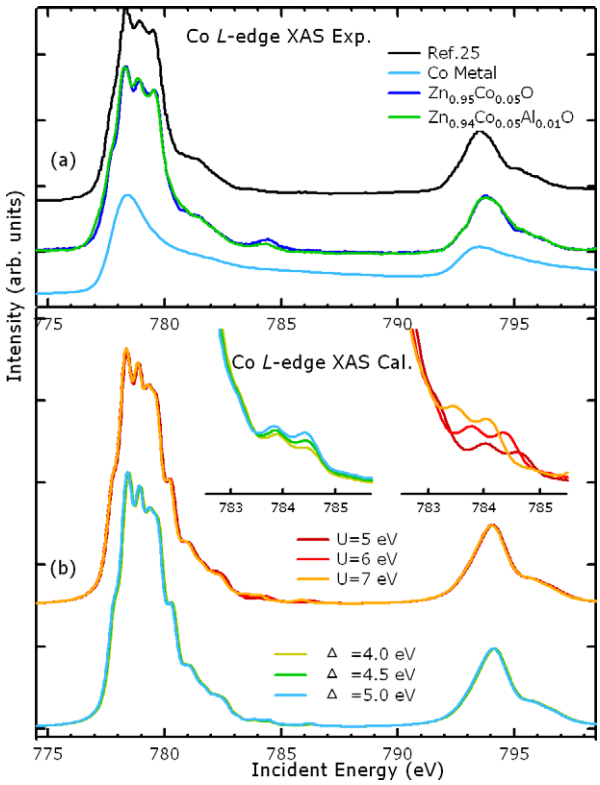

Figure 5. (a) Co-L XAS spectra of ZCO, ZCAO, $Zn_{0.9}Co_{0.1}O$ from [25] as well as Co metal. (b) The calculated XAS spectra under the influences of the charge transfer (CT) energy Δ and the Coulomb interaction energy U.

calculated results. It is noted that U has a slightly stronger influence than Δ, although both of them possibly contribute. However, we realize the difficulty in specifying the relative contribution from each by judging the weak CT structure of XAS spectra.

Therefore, we measured RIXS by detuning the incoming photon energy to the CT satellite. The spectrum is shown as RIXS G in figure 6. It is interesting to find CT intensity distinctly strengthens in ZCO, which is more pronounced than that in XAS spectra. However, the energy positions of the two CT peaks nearly superpose, being consistent with that shown in XAS. In addition to RIXS G, spectra excited at the L_3 white line and the pre-edge are also collected and presented as F and E respectively in figure 6. We compared the prominent difference of CT structures from E and plotted the details in the inset of the figure. The energy loss position of ZCAO is found about 0.6 eV higher than ZCO with an unchanged intensity.

In order to know which parameter governs the CT peak's intensity and/or energy position, we computed the RIXS spectral shape under the influence of the V, Δ and U parameters by again using CTM theory. Figure 7 depicts the calculated spectra under the excitations of E and G. We observe the parameter Δ varies the energy position of the CT peak in both of them. But V just modifies RIXS E's CT position, keeping the center of gravity of the other's constant. Having in mind the experimental spectra, we reveal that it is the V parameter other than Δ which dominates the CT spectral shape within the two samples. More explicitly, we found Co 3d

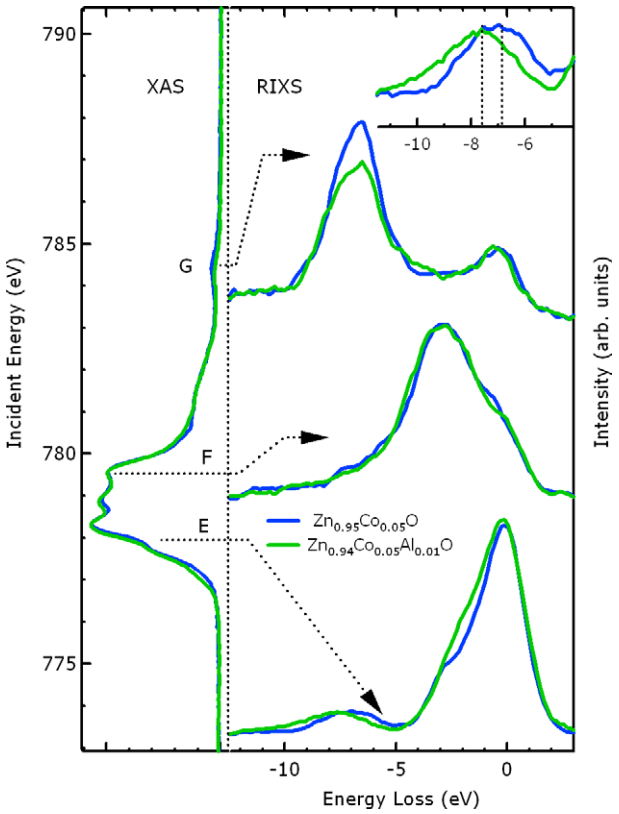

Figure 6. RIXS spectra of the Co-L when the excitation energy is detuned to position E, F and G as indicated in the left side of XAS spectrum. The inset at the top captures the details of the CT structure in RIXS E. The dashed lines mark the peak positions of CT structures.

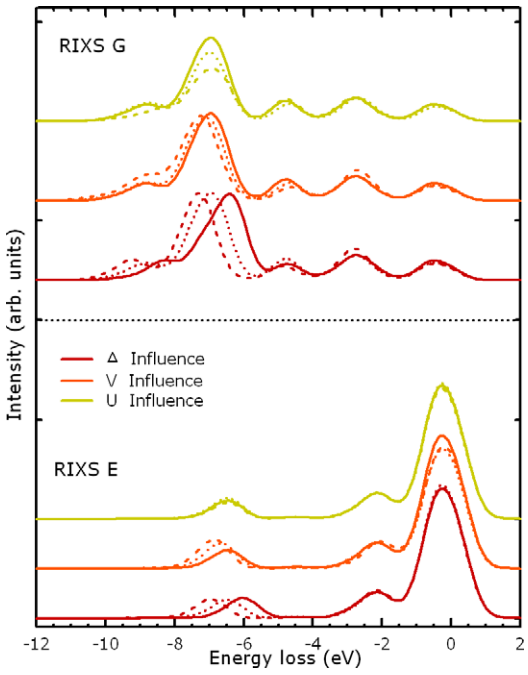

Figure 7. Calculated RIXS spectra under the influences of CT energy Δ (red), the hybridization strength V (orange), and the Coulomb interaction energy U (light green). For the CT influence RIXS, charge transfer energies $\Delta = 4.0$ eV (solid), 4.5 eV (dotted), and 5.0 eV (dashed) are used while keeping the hybridization energies of 0.8 eV and 1.0 eV for e_g and t_{2g} orbitals fixed. For the hybridization influence RIXS, V_{eg} varied from 0.8 (solid) to 1.0 (dotted) then 1.2 eV (dashed), and V_{t2g} from 1.0 to 1.2 then 1.4 eV, with Δ fixed to 4.5 eV. For the Coulomb interaction influence RIXS, U value is changed from 6 eV (solid), 4 eV (dotted) to 2 eV (dashed), where CT energy $\Delta = 4.5$ eV, and hybridization strengths (0.8 for e_g, and 1.0 for t_{2g} orbitals) are used.

states of ZCAO hybridize stronger with its O 2p states than ZCO does. This is nicely consistent with the results from XAS studies. For the CT intensity discrepancy in RIXS G, one notes it can be well accounted for by the Coulomb interaction U. As the high U value delivers a strong intensity of the CT peak, we thereby deduce ZCO has higher Coulomb interaction than ZCAO. The additional Al doping is figured out to reduce the on-site Coulomb interaction strength of Co ions in ZCAO. In fact, this result agrees with the Coulomb interaction influence on XAS spectra. We recall the definition of the metal–insulator transition (MIT) to explain this effect. It is known that the MIT is dominated by the relative magnitudes of the on-site Coulomb energy (U) and the one-electron bandwidth (W). The system prefers metallic behavior when $U/W \leqslant 1$ and insulating when $U/W \geqslant 1$. In our case, Al doping introduces free carriers resulting in the system which is more metallic like. Meanwhile, as the small additional Al cannot drastically change the bandwidth W, the weakening of the Coulomb interaction U is the most likely possibility to reduce the U/W ratio.

Our previous DFT calculations revealed the FM tends to stabilize in the ground state and the hybridization strength between Al 3p and Co 3d states weakens during Al substituting from site 1 to 6 [18]. However, the reason why the Al 3p and Co 3d states hybridization strength changes according to different Al doping sites is still unknown. We demonstrate that this question can be resolved by the present studies. Figure 8 depicts the number of the shared oxygen atoms between Al and Co tetrahedrons as well as the ground state energy difference between FM and AFM, i.e., $\Delta E_{\mathrm{FM-AFM}}$ (from [18]), according to different Al doping sites. As Co 3d hybridize with Al 3p states via the shared oxygen atoms in between, the less the shared oxygen atoms the weaker the hybridization strength of Co 3d and Al 3p states. Moreover, the weak hybridization releases an extra portion of free electrons doping into the conduction band of the ZnO host. These electrons on one hand, would rather act as free carriers and stabilize the FM state than localize around Co 3d orbitals, and facilitate the hybridization between O 2p and Co 3d/Al p states on the other. To quantitatively characterize the hybridization strength between oxygen and Co/Al ions, we utilize the a1/a2 intensity ratio. Its values as well as the number of shared oxygen atoms are listed in table 1. It manifests the intensity ratio of site 6 increases about 12% compared with site 1. Concerning the origin of the magnetic performance, we deduce it is the spatial distribution of Al, i.e., *various shared oxygen atoms*, rather than the direct distance between Co and Al ions. In table 1 we also provide the energy difference of FM and AFM ($\Delta E_{\mathrm{FM-AFM}}$), and the Co and Al ions' distance. The origin of the Co–Al ions' distance apparently breaks down since

Table 1. FM–AFM ground state energy difference, distance between Co and Al ions, a1/a2 intensity ratio in XAS and the shared oxygen numbers between Co and Al tetrahedrons for different Al defect configurations.

	Al doping site						
	1	2	3	4	5	6	Zn_{11}
ΔE_{FM-AFM} (meV)	+7	−10	−33	−48	−65	−64	
$d_{Co-Al\ ion}$ (Å)	3.250	3.209	3.209	5.086	5.673	6.138	6.903
a1/a2	0.92	0.96	1.01	1.03	1.05	1.04	1.04
Shared O numb	3	1	2	1	0	0	0

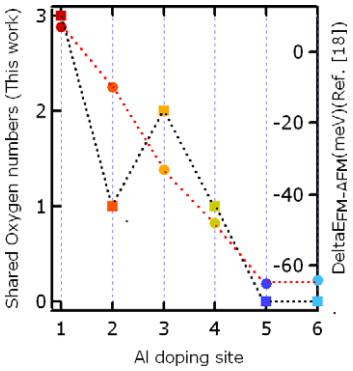

Figure 8. The number of shared oxygen atoms between Al and Co tetrahedrons (left), and the energy difference between FM and AFM state from [18] (right), when Al substitutes from site 1 to 6. The black and red dashed lines serve as guides to the eye.

ΔE_{FM-AFM} changes drastically while the distance keeps nearly constant during the Al doping from site 1 to 3. In order to further verify the origin of the Al defects' spatial distribution, the oxygen XAS spectra were calculated when Al substitutes the Zn_{11} site (see in figure 2). In this doping position, there is no shared oxygen atom but the distance between Co and Al is larger than that of site 6. The calculated XAS spectrum is plotted in figure 3. We find it is the same as that when Al in site 6. Hence, the Co and Al hybridization strength is regarded consistent as in site 6 though the Co and Al ion distance is about 0.77 Å larger than the latter. This result convinces us surely that the spatial distribution of the Al donor defect, rather than the distance between Co and Al ions, governs the different magnetic performances of the material.

4. Conclusion

To summarize, we have investigated the electronic structure of $Zn_{0.95}Co_{0.05}O$ and $Zn_{0.94}Co_{0.05}Al_{0.01}O$ nano-powders by combining XAS and RIXS studies on both the oxygen K- and Co L-edges as well as *ab initio* multiple scattering and multiplet calculations. Studies on the O K-edge reveal that Al defects induce various hybridization strengths between Al 3p (and/or Co 3d) and O 2p states when doping in different substitutional Zn sites. Particularly, we note the shared oxygen atoms between the local Al and Co tetrahedrons play a crucial role in the hybridization states which is responsible for different features in the oxygen XAS spectra and the ferromagnetic performances. Work on Co L-edges confirm the O 2p and Co 3d (and/or Al 3p) state hybridization strengthens when introducing Al donor defects. Moreover, the enhancement of the hybridization strength assists the electron hopping between the impurities and the host and in turn reduces the Co ion on-site Coulomb interaction energy. To be specific, we find the additional Al donor is crucial for the ferromagnetism in nano (Co, Al) co-doped powder. The magnetic difference of the material is better understood as being governed by the spatial distribution of Al, i.e., *various shared oxygen atoms*, rather than the distance between the Al defects and Co impurities.

Acknowledgments

This work was supported by the Natural Science Foundation of China at the Beijing Synchrotron Radiation Facility, Institute of High Energy Physics through Grant Nos 10775150 and 10435050. Experimental support by A Yagishita in Photon Factory is gratefully acknowledged. KJZ acknowledges fruitful discussions with Frank de Groot and P Glatzel, who provide him with the TT multiplet code and RIXS procedures. The theoretical work was supported by computing time at the Shanghai Supercomputing Center (SSC). KJZ also acknowledges stimulating discussions with C Hague, J Luening, G S Chuzbainan and B Watts.

References

[1] Ohno H 1998 *Science* **281** 951
[2] Dietl T, Ohno H, Matsukura F, Cibert J and Ferrand D 2000 *Science* **287** 1019
[3] Ueda K, Tabata H and Kawai T 2001 *Appl. Phys. Lett.* **79** 988
[4] Griffin K A, Pakhomov A B, Wang C M, Heald S M and Krishnan K M 2005 *Phys. Rev. Lett.* **94** 157204
[5] Guo J-H *et al* 2007 *J. Phys.: Condens. Matter* **19** 172202
[6] Li X L, Xu X H, Quan Z Y, Guo J F, Wu H S and Gehring G A 2009 *J. Appl. Phys.* **105** 103914
[7] Liu X C, Shi E W, Chen Z Z, Zhang H W, Xiao B and Song L X 2006 *Appl. Phys. Lett.* **88** 252503
[8] He Y, Sharma P, Biswas K, Liu E Z, Ohtsu N, Inada Y, Nomura M, Tse J S, Yin S and Jiang J Z 2008 *Phys. Rev.* B **78** 155202
[9] Ma Y W, Ding J, Yi J B, Zhang H T and Ng C M 2009 *J. Appl. Phys.* **105** 07C503
[10] Lee S, Cho Y C, Kim S-J, Cho C R, Jeong S-Y, Kim S J, Kim J P, Choi Y N and Sur J M 2009 *Appl. Phys. Lett.* **94** 212507
[11] Kim J H, Kim H, Kim D, Ihm Y E and Choo W K 2002 *J. Appl. Phys.* **92** 6066
[12] Lee E C and Chang K J 2005 *Phys. Rev.* B **69** 085205
[13] Ando K, Saito H, Jin Z W, Fukumura T, Kawasaki M, Matsumoto Y and Koinuma H 2001 *Appl. Phys. Lett.* **78** 2700
[14] Hsu H S, Huang J C A, Huang Y H, Liao Y F, Lin M Z, Lee C H, Lee J F, Chen S F, Lai L Y and Liu C P 2006 *Appl. Phys. Lett.* **88** 242507

[15] Liu X C *et al* 2008 *J. Phys.: Condens. Matter* **20** 025208
[16] Liu X C *et al* 2008 *Appl. Phys. Lett.* **92** 042502
[17] Pemmaraju C D, Hanafin R, Archer T, Braun H B and Sanvito S 2008 *Phys. Rev.* B **78** 054428
[18] Zhang T, Song L X, Chen Z Z, Shi E W, Liu X C and Zhang H W 2006 *Appl. Phys. Lett.* **89** 172502
[19] Yan Y L and Yagishita A 1995 *KEK Report* p 95
[20] Harada Y, Kinugasa T, Eguchi R, Matsubara M, Kotani A, Watanabe M, Yagishita A and Shin S 2000 *Phys. Rev.* B **61** 12854
[21] Chiou J W *et al* 2006 *Appl. Phys. Lett.* **89** 043121
[22] Ankudinov A L, Ravel B, Rehr J J and Conradson S D 1998 *Phys. Rev.* B **58** 7565
[23] Lee E-C and Chang K J 2004 *Phys. Rev.* B **69** 085205
[24] Preston A R H, Ruck B J, Piper L F J, DeMasi A, Smith K E, Schleife A, Fuchs F, Bechstedt F, Chai J and Durbin S M 2008 *Phys. Rev.* B **78** 155144
[25] Wi S C *et al* 2004 *Appl. Phys. Lett.* **84** 4233
[26] de Groot F 2001 *Chem. Rev.* **101** 1779
[27] Zhou K J *et al* 2009 submitted